

SCIENTIFIC REPORTS



OPEN

Ultrafast syn-eruptive degassing and ascent trigger high-energy basic eruptions

Marisa Giuffrida¹, Marco Viccaro^{1,2} & Luisa Ottolini³

Lithium gradients in plagioclase are capable of recording extremely short-lived processes associated with gas loss from magmas prior to extrusion at the surface. We present SIMS profiles of the ${}^7\text{Li}/{}^{30}\text{Si}$ ion ratio in plagioclase crystals from products of the paroxysmal sequence that occurred in the period 2011–2013 at Mt. Etna (Italy) in an attempt to constrain the final ascent and degassing processes leading to these powerful eruptions involving basic magma. The observed Li concentrations reflect cycles of Li addition to the melt through gas flushing, and a syn-eruptive stage of magma degassing driven by decompression that finally produce significant Li depletion from the melt. Modeling the decreases in Li concentration in plagioclase by diffusion allowed determination of magma ascent timescales that are on the order of minutes or less. Knowledge of the storage depth beneath the volcano has led to the quantification of a mean magma ascent velocity of ~ 43 m/s for paroxysmal eruptions at Etna. The importance of these results relies on the application of methods, recently used exclusively for closed-system volcanoes producing violent eruptions, to open-conduit systems that have generally quiet eruptive periods of activity sometimes interrupted by sudden re-awakening and the production of anomalously energetic eruptions.

Modes and timescales of magma ascent and degassing in the shallow portion of a volcano plumbing system (upper few kilometers) are crucial to understanding the dynamics of an eruption. The rate at which the magma rises to the surface controls the capability of magmas to lose the gas phase that in turn influences the effusive or explosive behavior of an eruption^{1,2}. Syn-eruptive ascent and decompression rates of magmas in explosive eruptions have been inferred through experimental simulation^{3,4} or from textural characteristics of the emitted products^{5–8}. However, direct measurements of ascent velocity during volcanic eruptions are not routinely constrained through *in-situ* analyses on minerals and melts. One obstacle to such kind of studies is that the ascent velocities of gas-rich magmas and their vesiculation upon eruption may be extremely fast (hours, minutes or even less), which makes them difficult to assess with standard geospeedometers, such as diffusion of elements in various minerals (Fe–Mg in olivine, Mg, Sr, Ba in plagioclase). Recent studies invoked the diffusion of volatile species between melt and bubbles as a new method to quantify magma ascent and decompression rates^{9–11}. Other methods involved the investigation of intra-crystalline diffusion of light elements, such as Li, Be and B that are markers of magma degassing^{12,13}. In particular, concentration gradients of Li in plagioclase crystals have proved to be useful for the identification and quantification of fast processes of magma ascent and degassing that occur shortly before, and even during eruptions^{12,14–17}. The increasing interest in studying Li concentrations and its diffusive processes is based on the observation of the extremely mobile behaviour of Li, which easily migrates into the fluid phase at low pressure¹⁸ with rates faster than those of water¹⁹. Moreover, the fluid–melt partition coefficient of Li increases with decreasing pressure¹⁸. The rates of Li diffusion in plagioclase are 10^{-10} – 10^{-12} m² s⁻¹ for a temperature range of 200–850 °C, i.e. orders of magnitude faster than NaSi–CaAl interdiffusion^{20–22}. This means that Li diffusion is sufficiently rapid to constrain short-lived magmatic processes, because any Li concentration gradient in plagioclase would be rapidly homogenised through diffusion to the equilibrium profile, unless arrested by sudden cooling of magma after emission¹². Lithium has been successfully used for time constraints of syn-eruptive degassing in volcanic systems erupting products of various compositions (basalts to rhyolite), whose degassing occurs primarily

¹Università di Catania, Dipartimento di Scienze Biologiche, Geologiche e Ambientali – Sezione di Scienze della Terra, Corso Italia 57, I-95129, Catania, Italy. ²Istituto Nazionale di Geofisica e Vulcanologia (INGV) - Sezione di Catania, Osservatorio Etneo, Piazza Roma 2, 95125, Catania, Italy. ³Consiglio Nazionale delle Ricerche (CNR), Istituto di Geoscienze e Georisorse (IGG) – Sezione di Pavia, Via A. Ferrata 1, I-27100, Pavia, Italy. Correspondence and requests for materials should be addressed to M.V. (email: m.viccaro@unict.it)

under closed-system conditions (e.g., Taupo, New Zealand; Volcàn de Fuego, Guatemala; Nea Kameni Santorini, Greece; Mt. St. Helens, USA).

We report here the results of Secondary Ion Mass Spectrometry (SIMS) investigations of Li in plagioclase crystals found in agglutinates and rheomorphic lava flows produced by Mt. Etna volcano during the violent paroxysms that occurred during the 2011–2013 AD period at the New South East Crater, and which were sampled and quenched immediately after the emplacement. The paroxysmal eruptions (44 episodes throughout 2011–2013 AD) considered in this study have been similar to each other regarding the composition of the erupted products and eruptive behaviour²³. During each paroxysmal eruption, the evolution of the volcanic phenomena was characterized by varying durations of an early weak- to mildly-Strombolian activity, shifting later to violent Strombolian activity and vigorous lava fountaining (~1-km-high above the crater edge) that produced eruptive columns up to several km high^{23,24}. The novelty of the present study arises from the application of Li diffusion modeling to unraveling the timescales of syn-eruptive decompression-driven degassing at Mt. Etna, which is generally acknowledged to degas through open-system conditions, but is also able to produce extremely energetic eruptions.

Analytical Procedures

Thin sections representative of agglutinates and rheomorphic lavas from various paroxysmal events occurred at Mt. Etna in the period 2011–2013 have been selected and prepared for the ion microprobe. SIMS investigations were performed on selected plagioclase crystals and on the matrix glass immediately adjacent to the selected crystals. Among plagioclase crystals preserved in lava rocks from the recent eruptive activity at Mt. Etna volcano, seven crystals were chosen because they are totally oscillatory-zoned plagioclases, indicating crystal growth close to equilibrium. The thin sections were polished, washed in an ultrasonic tank, and Pt-coated prior to SIMS analysis conducted using the IMS 4f Cameca ion microprobe installed at CNR-IGG (Pavia). We used a 5 nA $^{16}\text{O}^-$, 6–8 μm \varnothing primary beam to sputter secondary ions from micro-areas chosen along transects within the crystals and in the adjacent matrix glass. The analytical set up was as follows: –12.5 kV accelerating voltage, 25- μm secondary-ion imaged field, 400- μm contrast aperture, 1800- μm field aperture, and 900 (M/ Δ M) mass resolving power. The energy filtering technique of secondary ions (range: 75–125 eV) was adopted to reduce matrix effects and improve analytical precision^{25,26}. $^7\text{Li}^+$ and $^{30}\text{Si}^+$ were monitored over 5 analytical cycles with 8 and 4 sec acquisition time each - for a total time of 40 and 20 sec, respectively - after a 450-sec waiting time to obtain steady-state sputtering conditions. NIST-SRM-610, –612 and –614 international standards were used as calibration samples in order to convert the ion signal for Li into Li concentrations (ppm, wt.%)^{27,28}. The analytical reproducibility of the $^7\text{Li}^+ / ^{30}\text{Si}^+$ ratios resulted to be $\pm 1\%$ (1 σ) for NIST-SRM-610 over a day. The experimental data for all the crystals were collected in four, one-day analytical sessions. After SIMS investigations, the thin sections were then smoothly re-polished, and analysed at the Tescan Vega-LMU SEM (equipped with an EDAX Neptune XM4-60 micro-analyzer and coupled with an EDAX EDS and WDS LEXS spectrometer, calibrated for light elements), at Dipartimento di Scienze Biologiche, Geologiche e Ambientali (University of Catania) to determine major element composition and the proper anorthite content relative to each SIMS spot. Operating conditions were the following: 20 kV accelerating voltage, 2 nA beam current and ~2 μm \varnothing focused electron beam. Repeated analyses on internationally certified minerals and internal glass standards ensured precision for all the collected elements on the order of 3–5%.

The SEM-EDS/WDS SiO_2 (wt.%) values at each spot were finally adopted in the SIMS quantification of Li. Moreover, in order to further reduce the residual matrix effects and take into account the different SiO_2 (wt.%) values among the plagioclase crystals and the NIST glasses (~50 wt.% SiO_2 vs. 72.2 wt.% SiO_2 in the NIST-series glasses), we applied a correction to the relative-to-Si ion yield for Li, i.e., $I(\text{Li})/I(\text{Si}) / \text{Li}(\text{at})/\text{Si}(\text{at})$ [where $I(\text{Li})$ and $I(\text{Si})$ represent the ionic signals for Li and Si, and $\text{Li}(\text{at})$ and $\text{Si}(\text{at})$, their respective atomic concentrations]²⁵. The accuracy of the final SIMS data for Li concentration is quoted better than 10% rel. The anorthite composition determined at each SIMS spot was used to correct the measured $^7\text{Li}/^{30}\text{Si}$ ratios for the variation in silica. Specifically, the ^{30}Si count rate was converted into $^{30}\text{Si}_i$, which is proportional to the amount of plagioclase sputtered during the analysis. This conversion follows the equation:

$$^{30}\text{Si}_i = ^{30}\text{Si}\{(4/3) + 2X_{An}/3\} \quad (1)$$

where the $^{30}\text{Si}_i$ value accounts for the number of tetrahedral sites sputtered during SIMS bombardment, assuming constant ionization efficiency for Si^{17} . Therefore, the $^7\text{Li}/^{30}\text{Si}_i$ signal ratio represents a value proportional to the molar Li content within the plagioclase, i.e. proportional to the number of Li atoms for the tetrahedral site¹⁷.

Results and Discussion

Crystals used in this study are An_{72-90} plagioclases with sizes between ~500 and 950 μm . Only plagioclase 23Feb13_P6 represents an exception, as it is more Ab-rich than the other crystals (An_{56-68}) meaning that it may have experienced crystallization in a more differentiated melt. In general, anorthite variation throughout the core-to-rim profile is narrow (i.e. An oscillation range in the order of 5–10 mol%), and can show either slight increases or decreases at the outermost edge. In all crystals, Li concentration was measured as variations of the $^7\text{Li}/^{30}\text{Si}$ ion ratios along 200–300 μm -long transects that follow the apparent plagioclase *c*-axis. $^7\text{Li}^+ / ^{30}\text{Si}^+$ values range from 2.7×10^{-3} to 0.4×10^{-4} , corresponding to absolute Li concentrations between 6.8 ppm and 0.1 ppm (Fig. 1). It is worth noting that for this study we did not measure $^6\text{Li}/^7\text{Li}$ ratios, in spite of the potential for this ratio to be a good indicator for diffusion^{29,30}, because the counting rates at the mass of ^6Li were insufficient to produce robust counting statistics. Examinations of the Li SIMS profiles have shown overall trends of decreasing concentrations from the crystal interior toward the edge, without specific correlations to the An concentration profile of each crystal. Throughout the analysed spatial ranges, we also recognized localized spikes in the Li content that

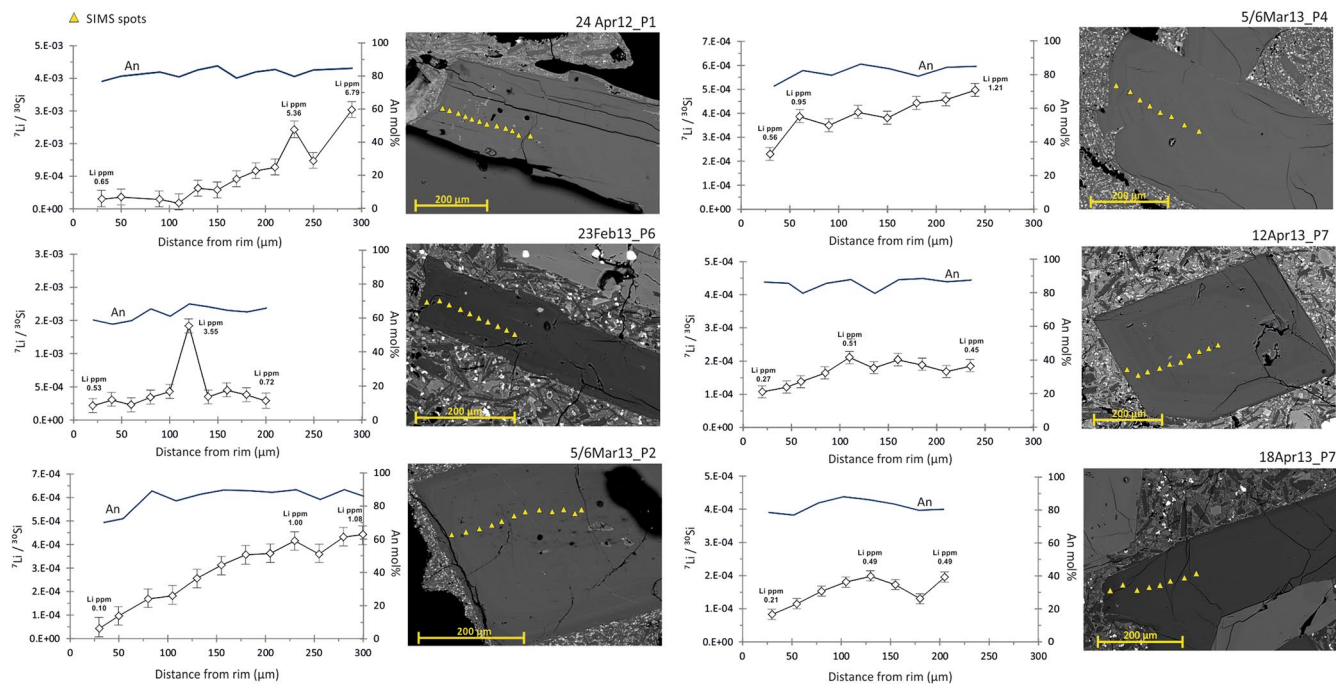


Figure 1. Ion microprobe analysis spots for ${}^7\text{Li}/{}^{30}\text{Si}$ (An-corrected) versus distance from crystals edge plotted together with the An mol% content (SEM-EDS/WDS analysis) for plagioclase crystals in this study. Error bars are the standard deviation of the mean of measurements ($\pm 1\sigma$).

shifts to higher values at rather regular intervals within the plagioclase (Fig. 1). SIMS measurements of the ${}^7\text{Li}/{}^{30}\text{Si}$ ratio in the matrix glass immediately adjacent to the analysed plagioclase crystals provide evidence of a significant variability in the Li concentration of the plagioclase host melt. Glass data indicate ${}^7\text{Li}/{}^{30}\text{Si}$ ion ratios of one-two orders of magnitude higher compared to values in plagioclase, corresponding to actual Li concentrations between 0.5 and 29 ppm.

Decreasing concentrations of Li toward the edge of plagioclase crystals have been interpreted as superimposition of the effect of mineral-melt partitioning and loss of Li from the melt due to preferential transport of Li into the gas phase during the eruption^{14–16}. Former experimental studies of plagioclase-melt partition coefficients demonstrate that Li is moderately incompatible in An_{39-77} plagioclase ($K_D = 0.15-0.7$) and that crystal-melt partition coefficient does not vary systematically with changing X_{An} at constant temperature^{31–33}. However, these experiments highlighted that the melt composition may play a role in controlling the partition coefficient of Li between crystals and melt. Indeed, more recent experiments proved that the partitioning of Li into plagioclase is a function of the An contents over the composition range $\text{An}_{60}-\text{An}_{89}$, decreasing of a factor of ~ 3.5 from An_{60} to An_{80} ³⁴. Anorthite variation of the Etnean crystals is, however, rather limited (ΔAn is only 5–10 mol%) and does not correlate with the decreasing Li profile. This implies that changes in Li partitioning behavior are unlikely to fully explain the observed depletion of Li towards the crystal rims. Moreover, the relatively homogeneous melts reported for the recent eruptive products of Etna²³ suggest that changes in the plagioclase/melt partition coefficient for Li due to compositional changes of the melt would be small, and insufficient to explain the observed concentration profiles. Unless the plagioclase crystals were mixed with a Li-poor magma during its final stages of growth, the general rim-wards decline of Li concentrations can be only interpreted as a consequence of diffusive Li disequilibrium related to volatile exsolution during magma ascent. Despite magma ascent and degassing paths for past eruptions of Mt. Etna being well constrained by several melt inclusion studies^{35–40}, the existence of a sufficiently low-Li magma beneath Etna that would explain the observed concentration profiles is not supported by measurements of Li in coexisting melt inclusions. The few data available indicate that Li contents in Etnean melt inclusions vary from 3.4–10.2 ppm for a wide range of eruptions that occurred in historic and recent times^{41–44}. In particular, melt inclusions entrapped in crystals of recent products at pressure lower than 300 MPa ($<7-10$ km b.s.l.)⁴⁴ have Li contents of 7.8–9.9 ppm, much higher than those measured in our plagioclase crystals. Given the incompatibility of Li in all mineralogical phases, the amount of Li should progressively increase in the residual melt through fractional crystallization. In this regard, the high Li concentration of the matrix glass confirms the absence of Li-poor melts in which crystals may have been stored for a given time, sufficient to produce the observed Li concentration gradients (see ESM1 in the Supplementary Information for compositions of matrix glasses). Excluding a major role played by Li-melt partitioning or the entrainment into a Li-poor magma volume, the observed decreases in Li in plagioclase crystals must reflect, therefore, rapid decreases in melt Li presumably due to ascent-driven degassing. This inference is robust considering that Li gradients have been measured only in oscillatory-zoned crystals, which are assumed to crystallize under rather unperturbed chemical and physical conditions. This should remove the potential contribution deriving from the superimposition of other pre-eruptive magmatic processes on the plagioclase Li concentration before the final stage of degassing. Our data also support

the idea that depletion of Li from the melt due to volatile exsolution was an incomplete process, as the ground-mass glass compositions are far too high in Li to be in equilibrium with the plagioclase Li contents.

The occurrence of localized Li spikes that are superimposed on the main trends of decreasing Li within the plagioclase requires an increase in Li abundance in the host melt. Compositional trends characterized by increasing Li toward the margin of plagioclase were previously observed during the investigation of products of the ~27 ka Oruanui eruption (Taupo, New Zealand), and interpreted as a consequence of changing Li partitioning behaviour due to extensive release of Cl from the system during decompression¹⁷. The discharge of a significant amount of Cl from a melt at subcritical fluid conditions was found to affect the partitioning of Li that forms LiOH hydroxides. This process would make Li far less compatible in the melt, increasing its chemical activity, and thus providing the driving force for Li diffusion back into plagioclase crystals¹⁷. Etnean trachybasalts are acknowledged to be volatile-rich, and the Cl concentration in the melt is significant, ranging between 0.05 and 0.46 wt.%^{37,38,40}. However, the preferential partitioning of Li into the melt driven by extensive loss of Cl cannot account for the development of localized Li peaks in these Etnean products. Indeed, the exsolution of a Cl-bearing volatile phase in Etnean magmas begins at ~100 MPa^{37,38,40} and becomes more prominent due to ascent-driven decompression. Therefore, if we assume that Cl exsolution effectively changes the Li partitioning, enhancing the preferential partitioning of Li back into the melt, this mechanism would produce a continuous trend of Li increase toward the plagioclase edge¹⁷, which is clearly in contrast with what we observed. Moreover, based on compositional observations on plagioclase crystals erupted during 2011 and 2013 at Mt. Etna, magmatic recharge and mixing events cannot be responsible for changes in melt Li contents, as fluctuations in minor elements such as Fe, Mg and/or Ti do not correlate with Li spikes²⁴. We believe that the observed short-length scale Li peaks within plagioclase crystals likely reflect transient dynamic processes associated with gas migration from deep portions of the Etna transport system. Published data on primitive glass inclusions in olivines confirm that the volatile-rich magmas of Mt. Etna can exsolve a H₂O-CO₂ gas phase at pressure higher than 250 MPa^{36–40}, which continuously flush the overlying magma reservoirs stored at lower pressure⁴⁵. These processes are thought responsible for the high explosivity of Etna eruptions in the past or during the last decades, as they act as a recurrent trigger mechanism for high-energy explosive events^{40,46–48}. In accordance with these observations, Li-bearing gases released from the deep levels of the volcano transport system may systematically rise up and accumulate in shallow reservoirs, where they partially re-equilibrate with the melt during storage, and hence serve to increase the Li content of the melt. Under these conditions, the longer a magma body is stored at low pressures, the greater the addition of Li to the melt^{14,49}. In spite of a lack of published data regarding Li distribution in melt inclusions to confirm the ascent of Li-rich gas phases at Mt. Etna, the occurrence of multiple peaks at higher Li concentration is likewise best explained via repeated cycles of gas flushing in shallow magma reservoirs, which are systematically recorded by plagioclase during its growth. The presence of short length scale Li spikes reflects heterogeneous compositions acquired by the crystal as a consequence of flushing before the final stage of degassing. Given that diffusion tends to erase any concentration gradient, this initial heterogeneity is also affected by diffusive relaxation. Preservation of Li spikes is therefore possible if diffusive relaxation due to final degassing is not complete, so that the crystal preserves a record of the initial heterogeneity that is superimposed on the main trend of Li decreasing toward the rim.

All the previous inferences support the development of plagioclase compositional profiles as expression of cycling addition and final diffusive relaxation of Li, which is a consequence of chemical disequilibrium between plagioclase and Li-depleted melt due to degassing. Modelling the diffusion of lithium in plagioclase provides us the opportunity to assess the timing of syn-eruptive decompression-driven degassing of magmas associated with the recent paroxysmal activity at Mt. Etna. We modelled each lithium profile using a one-dimensional model of diffusion in a semi-infinite solid, assuming uniform initial concentration in the crystal and constant concentration at the diffusion surface as initial and boundary conditions for the error function⁵⁰ (Fig. 2). The adopted approach allowed the derivation of analytical solutions for the following diffusion equation:

$$[(C_x - C_0)/(C_s - C_0)] = 1 - \text{erf}[x/2(Dt)^{0.5}] \quad (2)$$

where C_x represents the composition at the distance x from the surface, D is the diffusion coefficient for Li in plagioclase, and t is the time elapsed since diffusion begins. The diffusive evolution through time of Li was modelled with a composition-independent diffusion coefficient D of $3.04 \times 10^{-11} \text{ m}^2/\text{s}$, given the lack of correlation between the Li diffusion coefficient and major element concentrations in plagioclase²⁰. The concentration independence of the diffusion coefficient allowed using an analytical solution for the modelling, and thus we do not need to rely on more complex numerical solutions^{51,52}. Coefficients were calculated at 1080 °C by using the Arrhenius parameters (i.e., the pre-exponential factor D_0 , and the activation energy Q) for Li diffusivity in plagioclase of anorthitic composition²⁰. The choice of temperature is in accordance with the eruptive temperatures obtained at Mt. Etna by geothermometers calibrated for Etnean basalts⁵³. It is worth noting that Li diffusion coefficients in plagioclase have been experimentally calibrated only for the temperature range 200–850 °C²⁰. However, extrapolation of the coefficient for higher temperatures has been made possible due to the linear correlation between the $\log D_{\text{Li}}$ and temperature²⁰. Diffusion modelling calculations yielded average timescales of syn-eruptive magma ascent and degassing for the recent paroxysmal eruptions at Mt. Etna of 84 ± 10 seconds (Table 1). Our model led to the longest timescales for magmas feeding the eruption of March 5–6, 2013 (170 ± 21 to 183 ± 23 seconds), whereas significantly shorter timescales were estimated for the February 23, 2013 eruption (10 ± 1 seconds). Uncertainties on these timescales were calculated by propagating the error in the determination of diffusion coefficient D , through the relationship $t = x^2/4D$, where x^2 represents the diffusion length (in μm) within the profile, and t is the time⁵⁴. The uncertainty on D was calculated using standard procedures for error propagation in the Arrhenius expression, also taking into account uncertainties in the experimental determination of D_0 and Q for Li diffusivity in anorthite²⁰. Based on the error propagation analysis, the uncertainties on the calculated timescales are mainly

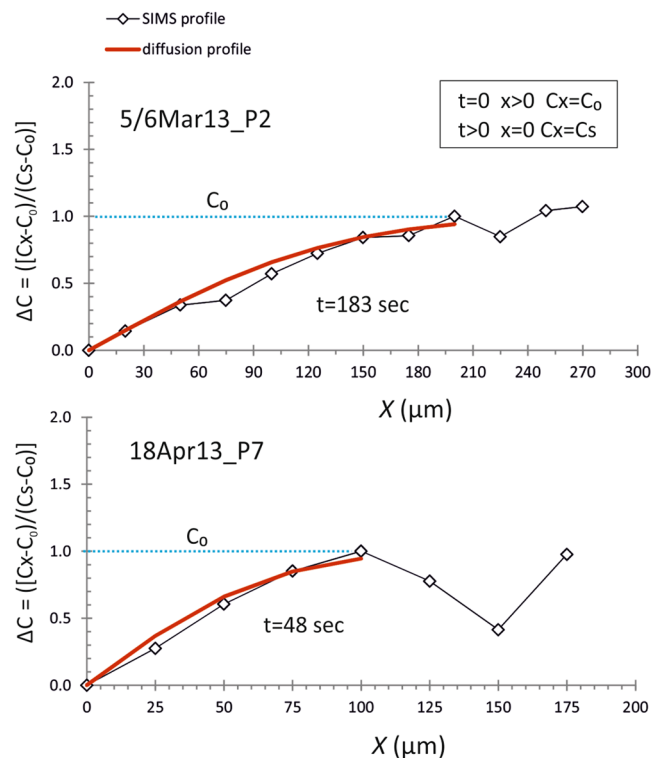


Figure 2. Examples of one-dimensional diffusion modeling application for Li profiles in Etnean plagioclase crystals. Light blue dashed lines indicate the initial concentration profile of the crystal (C_0), whereas the red lines represent the best-fit diffusion curves. ΔC (y -axes) refers to the normalized compositional contrast for Li in plagioclase. (see ESM2 in the Supplementary Information for all the modeled crystals).

Crystal	Eruption date	Diffusion width (μm)	Time (seconds)	2σ
24Apr12_P1	April 24, 2012	210	60	± 7
24Apr12_P3	April 24, 2012	150	82	± 10
23Feb13_P6	February 23, 2013	100	10	± 1
5/6Mar13_P2	March 5-6, 2013	200	183	± 23
5/6Mar13_P4	March 5-6, 2013	210	170	± 21
12Apr13_P7	April 12, 2013	90	38	± 5
18Apr13_P7	April 18, 2013	100	48	± 6

Table 1. Time estimates of the Li diffusion from concentration profiles in plagioclase crystals of recent eruptions at Mt. Etna. All timescales calculated for diffusivities D of $3.04 \times 10^{-11} \text{ m}^2/\text{s}$ at 1080°C .

governed by temperature changes, which largely affect D , in a way that a temperature of $1080 \pm 10^\circ\text{C}$ produces a propagating uncertainty in timescales from ± 0.2 to ± 20 seconds.

These time estimates offer us the opportunity to determine the final rates of magma degassing and ascent associated with paroxysmal eruptions at Mt. Etna. Determinations of the ascent rate upon eruption require, however, some constraints on the pressure at which Li disequilibrium begins and, therefore, the pressure at which the magma was stored before eruption. In this regard, the compositional and textural characteristics of plagioclase crystals from the post-2011 activity at Mt. Etna highlighted common late-stage histories of crystallization in a shallow storage zone^{24,55,56}. This magma reservoir was inferred to be located below the summit area at 1.5–2 km a.s.l., corresponding to a pressure of $\sim 40 \text{ MPa}$ ^{57,58}. This indicates that just prior to the eruption, magmas were likely stored at an average depth of $\sim 1.6 \text{ km}$ beneath the volcano summit, and later underwent instantaneous decompression through the conduit. Assuming that the Li diffusion begins at this depth, our timescales imply average rates of final magma ascent on the order of 43 m/s for the considered highly explosive episodes at Mt. Etna. These ascent velocities for Etnean magmas are in the same range of rates estimated through diffusion modelling for a number of extremely powerful eruptions worldwide (4–64 m/s). The crucial findings of this study demonstrate that re-activation of the magmatic systems at open-conduit, basaltic volcanoes can occur with exceptionally fast timescales, which are on the whole comparable with those for syn-eruptive degassing derived for other closed-system volcanoes erupting on Earth, and is followed by the generation of highly energetic eruptions.

References

- Cashman, K. V. Volatile controls on magma ascent and eruption. In: Sparks, R. S. J. & Hawkesworth C. J. (Eds), *State of the Planet: Frontiers and Challenges in Geophysics*, 109–124 (2004).
- Rutherford, M. J. Magma ascent rates. In: Putirka, K. D. & Tepley, F. J., III (Eds), *Minerals, Inclusions and Volcanic Processes*. Mineralogical Society of America and Geochemical Society, *Reviews in Mineralogy and Geochemistry* **69**, 241–271 (2008).
- Rutherford, M. J. & Hill, P. M. Magma ascent rates from amphibole breakdown: an experimental study applied to the 1980–1986 Mount St. Helens eruptions. *J. Geophys. Res.* **98**, 19667–19685 (1993).
- Takeuchi, S., Tomiya, A. & Shinohara, H. Degassing conditions for permeable silicic magmas: implications from decompression experiments with constant rates. *Earth Planet. Sci. Lett.* **283**, 101–110 (2009).
- Klug, C., Cashman, K. V. & Bacon, C. Structure and physical characteristics of pumice from the climactic eruption of Mount Mazama (Crater Lake), Oregon. *Bull. Volcanol.* **64**, 486–501 (2002).
- Toramaru, A. BND (bubble number density) decompression rate meter for explosive volcanic eruptions. *J. Volcanol. Geotherm. Res.* **154**, 303–316 (2006).
- Shea, T. *et al.* Linking experimental and natural vesicle textures in Vesuvius 79AD white pumice. *J. Volcanol. Geotherm. Res.* **192**, 69–84 (2010).
- Miwa, T. & Geshi, N. Decompression rate of magma at fragmentation: Inference from broken crystals in pumice of vulcanian eruption. *J. Volcanol. Geotherm. Res.* **228**, 76–84 (2012).
- Liu, Y., Anderson, A. T. & Wilson, C. J. N. Melt pockets in phenocrysts and decompression rates of silicic magmas before fragmentation. *J. Geophys. Res.* **112**, B06204 (2007).
- Humphreys, M. C. S., Menand, T., Blundy, J. D. & Klimm, K. Magma ascent rates in explosive eruptions: constraints from H₂O diffusion in melt inclusions. *Earth Planet. Sci. Lett.* **270**, 25–40 (2008).
- Lloyd, A. S. *et al.* NanoSIMS results from olivine-hosted melt embayments: Magma ascent rate during explosive basaltic eruptions. *J. Volcanol. Geotherm. Res.* **283**, 1–18 (2014).
- Cabato, J., Altherr, R., Ludwig, T. & Meyer, H. P. Li, Be, B concentrations and ⁸⁷Li values in plagioclase phenocrysts of dacite from Nea Kameni (Santorini, Greece). *Contrib. Mineral. Petrol.* **165**, 1135–1154 (2013).
- Neave, D. A., Hartley, M. E., MacLennan, J., Edmonds, M. & Thordarson, T. Volatile and light lithophile elements in high-anorthite plagioclase-hosted melt inclusions from Iceland. *Geochim. Cosmochim. Acta* **205**, 100–118 (2017).
- Kent, A. J. R. *et al.* Vapor transfer prior to the October 2004 eruption of Mount St. Helens, Washington. *Geology* **35**, 231–234 (2007).
- Genareau, K., Clarke, A. B. & Hervig, R. L. New insight into explosive volcanic eruptions: connecting crystal-scale chemical changes with conduit-scale dynamics. *Geology* **37**, 367–370 (2009).
- Genareau, K. & Clarke, A. B. *In situ* measurements of plagioclase growth using SIMS depth profiles of ⁷Li/³⁰Si: a means to acquire crystallization rates during short duration decompression events. *Am. Mineral.* **95**, 592–601 (2010).
- Charlier, B. L. A. *et al.* Lithium concentration gradients in feldspar and quartz records the final minutes of magma ascent in an explosive supereruption. *Earth Planet. Sci. Lett.* **319**, 218–227 (2012).
- Webster, J. D., Holloway, J. R. & Hervig, R. L. Partitioning of lithophile trace elements between H₂O and H₂O+CO₂ fluids and topaz rhyolite melt. *Econ. Geol.* **84**, 116–134 (1989).
- Richter, R. M., Davis, A. M., De Paolo, D. J. & Watson, E. B. Isotope fractionation by chemical diffusion between molten basalts and rhyolite. *Geochim. Cosmochim. Acta* **67**, 3905–3923 (2003).
- Giletti, B. J. & Shanahan, T. M. Alkali diffusion in plagioclase feldspar. *Chem. Geol.* **139**, 3–20 (1997).
- Grove, T. L., Baker, M. B. & Kinzler, R. J. Coupled CaAl–NaSi diffusion in plagioclase feldspar: experiments and applications to cooling rate speedometry. *Geochim. Cosmochim. Acta* **48**, 2113–2121 (1984).
- Liu, M. & Yund, R. A. NaSi–CaAl interdiffusion in plagioclase. *Am. Mineral.* **77**, 257–283 (1992).
- Viccaro, M., Calcagno, R., Garozzo, I., Giuffrida, M. & Nicotra, E. Continuous magma recharge at Mt. Etna during the 2011–2013 period controls the style of volcanic activity and compositions of erupted lavas. *Mineral. Petrol.* **109**, 67–83 (2015).
- Giuffrida, M. & Viccaro, M. Three years (2011–2013) of eruptive activity at Mt. Etna: working modes and timescales of the modern volcano plumbing system from micro-analytical studies of crystals. *Earth Sci. Rev.* **171**, 289–322 (2017).
- Ottolini, L., Bottazzi, P. & Vannucci, R. Quantification of Lithium, Beryllium and Boron in Silicates by Secondary Ion Mass Spectrometry Using Conventional Energy Filtering. *Anal. Chem.* **65**, 1960–1968 (1993).
- Ottolini, L., Camara, F., Hawthorne, F. C. & Stirling, J. SIMS matrix effects in the analysis of light elements in silicate minerals: Comparison with SREF and EMPA data. *Amer. Mineral.* **87**, 1477–148 (2002).
- Gao, S. *et al.* Determination of Forty Two Major and Trace Elements in USGS and NIST SRM Glasses by Laser Ablation-Inductively Coupled Plasma-Mass Spectrometry. *Geostand. Newslet.: The Journal of Geostandards and Geoanalysis* **26**, 181–196 (2002).
- Pearce, N. J. G. *et al.* Compilation of new and published major and trace element data for NIST SRM 610 and NIST SRM 612 glass reference materials. *Geostand. Newslet.: The Journal of Geostandards and Geoanalysis* **21**, 115–141 (1997).
- Richter, F. M., Davis, A. M., De Paolo, D. J. & Watson, E. B. Isotope fractionation by chemical diffusion between molten basalts and rhyolite. *Geochim. Cosmochim. Acta* **67**, 3905–3923 (2003).
- Richter, F. M. *et al.* Isotope fractionation of Li and K in silicate liquids by Soret diffusion. *Geochim. Cosmochim. Acta* **138**, 136–145 (2014).
- Blundy, J. Experimental study of a Kiglapait marginal rock and implications for trace element partitioning in layered intrusions. *Chem. Geol.* **141**, 73–92.
- Bindeman, I. N., Davis, A. M. & Drake, M. J. Ion microprobe study of plagioclase basalt partition experiments at natural concentration levels of trace elements. *Geochim. Cosmochim. Acta* **62**, 1175–1193 (1998).
- Bindeman, I. N. & Davis, A. M. Trace element partitioning between plagioclase and melt: investigation of dopant influence on partition behavior. *Geochim. Cosmochim. Acta* **64**, 2863–2878 (2000).
- Coogan, L. A. Preliminary experimental determination of the partitioning of lithium between plagioclase crystals of different anorthite contents. *Lithos* **125**, 711–715 (2011).
- Métrich, N. & Rutherford, M. J. Low Pressure Crystallization Paths of H₂O-Saturated Basaltic-Hawaiitic Melts from Mt Etna: Implications for Open-System Degassing of Basaltic Volcanoes. *Geochim. Cosmochim. Acta* **62**, 1195–1205 (1998).
- Métrich, N., Allard, P., Spillaert, N., Andronico, D. & Burton, M. R. 2001 flank eruption of the alkali- and volatile-rich primitive basalt responsible for Mount Etna's evolution in the last three decades. *Earth Planet. Sci. Lett.* **228**, 1–17 (2004).
- Spillaert, N., Allard, P., Métrich, N. & Sobolev, A. V. Melt inclusions record of the conditions of ascent, degassing and extrusion of volatile-rich alkali basalt during the powerful 2002 flank eruption of Mount Etna (Italy). *J. Geophys. Res., Solid Earth* **111**, B04203 (2006a).
- Spillaert, N. & Métrich, N. Allard, P. S–Cl–F degassing pattern of water-rich alkali basalt: Modelling and relationship with eruption styles on Mount Etna volcano. *Earth Sci. Rev.* **248**, 772–786 (2006b).
- Collins, S. J., Pyle, D. M. & MacLennan, J. Melt inclusions track pre-eruption storage and dehydration of magmas at Etna. *Geology* **37**, 571–574 (2009).
- Moretti, R. *et al.* Degassing vs. eruptive styles at Mt. Etna volcano (Sicily, Italy). Part I: Volatile stocking, gas fluxing, and the shift from low-energy to highly explosive basaltic eruptions. *Chem. Geol.* <https://doi.org/10.1016/j.chemgeo.2017.09.017> (2017).
- Schiano, P., Clocchiatti, R., Ottolini, L. & Busà, T. Transition of Mount Etna lavas from a mantle-plume to an island-arc magmatic source. *Nature* **412**, 900–904 (2001).

42. Kamenetsky, V. S. *et al.* Arrival of extremely volatile-rich high-Mg magmas changes explosivity of Mount Etna. *Geology* **35**, 255–258 (2007).
43. Schimmelpfennig, I. *et al.* Calibration of cosmogenic ³⁶Cl production rates from Ca and K spallation in lava flows from Mt. Etna (38°N, Italy) and Payun Matru (36°S, Argentina). *Geochim. Cosmochim. Acta* **75**, 2611–2632 (2011).
44. Schiavi, F. *et al.* Geochemical heterogeneities in magma beneath Mount Etna recorded by 2001–2006 melt inclusions. *Geochem. Geophys. Geosyst.* **16**, 2109–2126 (2015).
45. Giuffrida, M., Holtz, F., Vetere, V. & Viccaro, M. Effects of CO₂ flushing on crystal textures and compositions: experimental evidence from recent K trachybasalts erupted at Mt. Etna. *Contrib. Mineral. Petrol.* **172**, 90 (2017).
46. Aiuppa, A. *et al.* Forecasting Etna eruption by real time evaluation of volcanic gas composition. *Geology* **35**, 1115–1118 (2007).
47. Aiuppa, A. *et al.* Terminal Strombolian activity at Etna's central craters during summer 2012: the most CO₂-rich volcanic gas ever recorded at Mount Etna. *Geochem. Journal* **50**, 123–138 (2016).
48. Nicotra, N. & Viccaro, M. Transient uprise of gas and gas-rich magma batches fed the pulsating behaviour of the 2006 eruptive episodes at Mt. Etna volcano. *J. Volcanol. Geotherm. Res.* **227–228**, 102–118 (2012).
49. Berlo, K. *et al.* Geochemical precursors to volcanic activity at Mount St. Helens, USA. *Science* **306**, 1167–1169 (2004).
50. Crank, J. *The mathematics of diffusion* (Oxford Univ. Press, London, 1967).
51. Costa, F., Dohmen, R. & Chakraborty, S. Time scales of magmatic processes from modeling the zoning patterns of crystals. *Review in Mineralogy and Geochemistry* **69**, 545–594 (2008).
52. Costa, F. & Morgan, D. Time constraints from chemical equilibration in magmatic crystals. In: Dosseto, A., Turner, S. P., Van Orman, J. A. (eds) *Timescales of magmatic processes: from core to atmosphere*. Wiley, Oxford, 125–159 (2010).
53. Pompilio, M., Trigila, R. & Zanon, V. Melting experiments on Mt. Etna lavas: I - The calibration of an empirical geothermometer to estimate the eruptive temperature. *Acta Vulcanol.* **10**, 67–75 (1998).
54. Kahl, M., Chakraborty, S., Pompilio, M. & Costa, F. Constraints on the nature and evolution of the magma plumbing system of Mt. Etna volcano (1991–2008) from a combined thermodynamic and kinetic modelling of the compositional record of minerals. *J. Petrol.* **56**, 2025–2068 (2015).
55. Viccaro, M., Garozzo, I., Cannata, A., Di Grazia, G. & Gresta, S. Gas burst vs. gas-rich magma recharge: a multidisciplinary study to reveal factors controlling triggering of the recent paroxysmal eruptions at Mt. Etna. *J. Volcanol. Geotherm. Res.* **278–279**, 1–13 (2014).
56. Viccaro, M. *et al.* Crystal residence time from trace element zoning in plagioclase reveal changes in magma transfer dynamics at Mt. Etna during the last 400 years. *Lithos* **248**, 309–323 (2016).
57. Patané, D. *et al.* Insight into magma and fluid transfer at Mount Etna by a multiparametric approach: A model of the events leading to the 2011 eruptive cycle. *J. Geophys. Res. Solid Earth* **118**, 3519–3539 (2013).
58. Viccaro, M., Zuccarello, F., Cannata, A., Palano, M. & Gresta, S. How a complex basaltic volcanic system works: Constraints from integrating seismic, geodetic, and petrological data at Mount Etna volcano during the July–August 2014 eruption. *J. Geophys. Res. Solid Earth* **121**, 5659–5678 (2016).

Acknowledgements

M. Giuffrida acknowledges the PhD fellowship and two PhD research grants from the University of Catania. This work was supported by the funding programs of the University of Catania through the FIR 2014 grant number 2F119B and PRA 2016–18 cod. 22722132120 (Project Coordinator M. Viccaro). Draft of the manuscript benefited from the critical reviews by W.A. Bohrsen and R. De Rosa. We are also greatly thankful to A. Aiuppa for his editorial handling and to two anonymous reviewers who contributed to improve the submitted version of the manuscript.

Author Contributions

Marisa Giuffrida and Marco Viccaro conceived, wrote the main manuscript text and prepared the figures/table; Luisa Ottolini ran the SIMS analyses and provided data elaboration and quantification.

Additional Information

Supplementary information accompanies this paper at <https://doi.org/10.1038/s41598-017-18580-8>.

Competing Interests: The authors declare that they have no competing interests.

Publisher's note: Springer Nature remains neutral with regard to jurisdictional claims in published maps and institutional affiliations.



Open Access This article is licensed under a Creative Commons Attribution 4.0 International License, which permits use, sharing, adaptation, distribution and reproduction in any medium or format, as long as you give appropriate credit to the original author(s) and the source, provide a link to the Creative Commons license, and indicate if changes were made. The images or other third party material in this article are included in the article's Creative Commons license, unless indicated otherwise in a credit line to the material. If material is not included in the article's Creative Commons license and your intended use is not permitted by statutory regulation or exceeds the permitted use, you will need to obtain permission directly from the copyright holder. To view a copy of this license, visit <http://creativecommons.org/licenses/by/4.0/>.

© The Author(s) 2017